Hollow optical waveguide devices and systems

R M Jenkins, B J Perrett, M E McNie, E D Finlayson, R R Davies, J Banerji and A R Davies
QinetiQ, St Andrews Road, Malvern, Worcestershire, U.K., WR14 3PS.

ABSTRACT

Hollow optical waveguides have some unique properties compared with their solid core counterparts. These include very broad waveband, high power transmission characteristics in conjunction with extremely low interfacing and propagation losses. Such characteristics provide considerable potential for novel electro-optic and infrared devices and systems. In conjunction with discrete micro-optical components hollow waveguides have been used to demonstrate integrated circuits which are the optical analogue of the electronic PCB. The underlying physics and technology of hollow optical waveguides will be discussed in the context of a wide range of applications.

Keywords: optical waveguides, hollow waveguides, integrated optics, multimode interference (MMI) devices.

1. INTRODUCTION

Hollow waveguides have fundamentally different propagation characteristics to solid core waveguides. The hollow core leads to transmission characteristics close to that of the atmosphere whilst still providing light guidance. As a consequence the operational waveband is significantly broader than for a solid core waveguide, as is the optical power density which can be supported before damage occurs. Furthermore, there is no refractive index interface between free-space and the hollow core, so there is no interface reflection or loss. As a result it is easy to integrate discrete components into a hollow waveguide circuit. An additional difference is that hollow waveguides inherently have a multimode nature, i.e. they cannot be designed to just support the propagation of the fundamental mode. Rather than being a disadvantage, as will be come clear, this has some significant advantages. Even though hollow waveguides have a multimode nature they can very effectively propagate high fidelity fundamental mode fields. Some of the fundamental properties of hollow waveguides are now described and their application to both systems and devices discussed.

2. HOLLOW WAVEGUIDE THEORY

Figure 1 illustrates a square cross-section hollow core waveguide. The multimode nature of the waveguide means that it supports the low loss propagation of a range of higher order linearly polarized EH_{pq} modes in addition to the fundamental mode (EH_{11}).

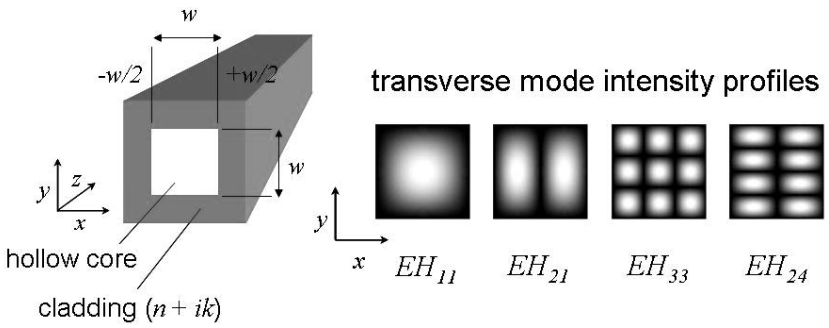

Figure 1. Schematic of a square cross-section hollow waveguide. In practice all the square cross-section hollow waveguides described in this paper are formed from a square section channel in conjunction with a lid. The transverse field intensity profiles on the right hand side clarify the mode nomenclature for the linear polarized EH_{pq} modes of the guide. The mode numbers p and q relate to the number of intensity maxima along the x and y axes respectively.

The complex transverse field amplitude of the EH_{pq} mode is given by the expression [1,2]:

$$EH_{pq}(x,y,z) = \frac{2}{w}\frac{cos}{sin}\left(\frac{p\pi x}{w}\right)\frac{cos}{sin}\left(\frac{q\pi y}{w}\right)exp(\gamma_{pq}z) \qquad (1)$$

Electro-Optical and Infrared Systems: Technology and Applications V, edited by David A. Huckridge, Reinhard R. Ebert
Proc. of SPIE Vol. 7113, 71130E · © 2008 SPIE · CCC code: 0277-786X/08/$18 · doi: 10.1117/12.802454

This expression assumes mode propagation along the z-axis of the waveguide which runs through the point $x = y = 0$ in the transverse x-y plane. The inner walls of the waveguide are located at the points $-w/2$ and $+w/2$ along the x and y axes respectively. In (1) we take the cosine function when p or q is odd and the sine function when p or q is even. Figure 1 illustrates some transverse intensity profiles (i.e. $|EH_{pq}(x,y,0)|^2$) for a range of low order modes. It is clear that the fundamental EH_{11} mode, has a quasi-Gaussian characteristic. The exponential term in expression (1) defines how the amplitude and phase of the EH_{pq} mode varies as a function of the axial propagation distance z according to the complex propagation constant γ_{pq}, which is given by the expression:

$$\gamma_{pq} = -\alpha_{pq} + i\beta_{pq} \qquad (2)$$

Here α_{pq} and β_{pq} are the attenuation and phase coefficients respectively, and are given by:

$$\alpha_{pq} = \frac{\lambda^2}{w^3}\left[p^2\, Re\left(\frac{1}{\left\{ (n-ik)^2 - 1 \right\}^{1/2}} \right) + q^2\, Re\left(\frac{(n-ik)^2}{\left\{ (n-ik)^2 - 1 \right\}^{1/2}} \right) \right] \qquad (3)$$

and,

$$\beta_{pq} = \frac{2\pi}{\lambda}\left[1 - \frac{1}{2}\left\{ \left(\frac{p\lambda}{2w} \right)^2 + \left(\frac{q\lambda}{2w} \right)^2 \right\} \right] \qquad (4)$$

In expressions (3) and (4), λ is the free-space wavelength of the propagating radiation and $n - ik$ is the complex refractive index of the inner walls of the waveguide. Alternatively, $n - ik$, can represent the effective complex index of a single or multi-layer coating applied to the inner walls of the hollow waveguide. The phase coefficient of the EH_{pq} mode β_{pq} given equation (4) is an approximation known as the "paraxial approximation" it leads to some unique self-imaging and field splitting properties in multimode waveguides as will be described later in the paper.

The power transmission for the EH_{pq} mode through a waveguide of length L is given as exp $(-2\alpha_{pq}L)$. Some consideration of equation (3) leads to the conclusion that for a given operational wavelength, λ, the attenuation coefficient for any given EH_{pq} mode can be made small simply by making the waveguide width w suitably large in comparison with the mode number. The lowest loss is always achieved for the fundamental mode but the higher order modes are not cut-off they are just more highly attenuated. As noted earlier, although this means that the waveguides have a multimode in nature, when manufactured to be rigid and linear in a suitable substrate, the optical transmission properties of such waveguides are much more controllable than those of multimode fibres. For example, with an appropriate input field it is possible to solely excite the fundamental mode or to excite a controlled spectrum of higher order modes. In this context, figure 2 illustrates calculations of the mode excitation that occurs when a TEM_{00} input beam is symmetrically injected into a square cross-section hollow waveguide.

In figure 2 the modal power coupling coefficient (the amount of power coupled to a given mode) is plotted as a function of the ratio of the diameter ($2\omega_0$) of the TEM_{00} input beam at its waist, to the hollow waveguide width, w. The calculations assume that the waist of the TEM_{00} beam is coincident with the entrance plane of the hollow waveguide and is accurately aligned with it. The predictions in figure 2 illustrate how the degree of power coupled to the different waveguide modes varies as a function of the ratio $2\omega_0/w$. The calculations were undertaken for all symmetric modes from $p = 1$ to 5, and $q = 1$ to 5, respectively. The lowest order mode considered is EH_{11} and the highest EH_{55}. With a value of $2\omega_0/w = 0.703$ the fundamental mode power coupling coefficient has a maximum value of 0.979, i.e. ~ 98% of the power in the TEM_{00} beam is coupled to the fundamental (EH_{11}) mode of the hollow waveguide with ~ 1% of the power coupled into a range of higher order modes and a further ~ 1% lost due to aperturing at the guide entrance.

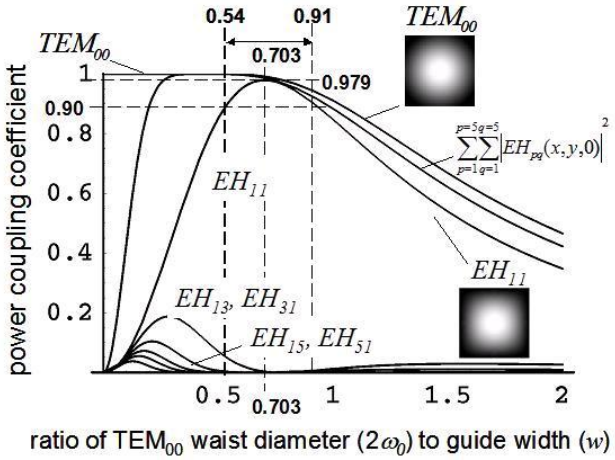

Figure 2. Theoretical predictions of the power coupling coefficient $|EH_{pq}(x,y,0)|^2$ for the modes p = 1 to 5, and q = 1 to 5, as a function of the ratio of the TEM_{00} input beam waist diameter ($2\omega_0$) to the guide width (w). For $(2\omega_0)/w$ = 0.0703, 98% of the power in the TEM_{00} is coupled to the fundamental (EH_{11}) waveguide mode.

For values of $2\omega_0/w$ smaller than 0.703 an increasing amount of power is coupled to higher order modes in turn. Specific choices of the magnitude of $2\omega_0/w$ lead to a controllable excited mode spectrum. For values of $2\omega_0/w$ greater than 0.703 the power coupled to the waveguide is reduced due to a combination of aperturing at the guide entrance and coupling to higher order modes. The form of the overlap integrals used in the calculations leads to the conclusion that the power coupled from a TEM_{00} beam to the fundamental waveguide mode, and the power coupled from the fundamental waveguide mode to a TEM_{00} beam, are equal in magnitude. As a result, the total TEM_{00} beam throughput, i.e. the power transmission from input to output, for a value of $2\omega_0/w$ = 0.703, is ~ 0.98^2 = 0.96, i.e. the power in a TEM_{00} input beam is transmitted with ~ 96% efficiency. This assume zero waveguide attenuation for the fundamental mode. Very low attenuation coefficients are achievable in reality. On the basis of calculations of the form described, we have conceived and demonstrated a wide range of hollow waveguide based systems and devices. The systems utilize the fact that fundamental mode fields can be efficiently launched an propagated, whereas the devices have made use of some of the unique properties of multimode propagation phenomena. The latter are based on meeting the ”paraxial approximation” criteria. Some examples of both systems and devices are now described in more detail.

3. HOLLOW WAVEGUIDE SYSTEMS

A good example of the use of hollow waveguide circuits for realising compact, rugged, high performance electro-optic systems is illustrated in figure 3. This shows a photograph of a subsystem for a 10.6 μm Range-Doppler imaging lidar [3]. The subsystem is based on the use of 2.0 mm wide hollow waveguides formed in the surface of a polycrystalline alumina substrate to guide 10.6 μm radiation through a circuit of eleven discrete optical components. The waveguides, and the deeper alignment slots for the components, were created by precision computer controlled milling techniques. As is clear from the photograph, the optical circuit is composed of linear sections of hollow waveguide interconnected by transmitting or reflecting components. A lid formed the fourth upper wall of all the hollow waveguides in question. In addition to the appropriate choice of diameter and alignment of the TEM_{00} input beam, relevant angular and lateral alignment tolerances were also defined and attained in practice for the integrated discrete components. These ensured that good fundamental mode coupling fidelity was achieved in coupling from one section of linear waveguide to another via a transmitting or reflecting component. The required angular and lateral alignment tolerances were defined as, $\theta \leq \lambda/5w$, and, $\gamma \leq w/10$, respectively. These ensured ≥ 0.95 (–0.2 dB) fundamental mode power coupling efficiency at any intersection [4]. These tolerances were achieved in practice by working to analogous tolerances on the angular and lateral alignments of the waveguides and component alignment slots in the waveguide circuit and to prescribed accuracies on the dimensional differences between the alignment slot widths and the component thicknesses. The parallelism of the faces of the optical components were also suitably defined. Although appropriate tolerances had to be met in practice in order to ensure efficient optical performance, the fact that the light is guided between the components in the hollow waveguide circuit, significantly eases the tolerances that are required compared with the analogous free-space situation.

The use of alignment slots to locate and align components also makes manufacture much easier than in the conventional approach where multiaxial tilt and translation stages are used to mount and align each component. The use of such mounts tends to make systems more bulky and more sensitive to misalignment than comparable hollow waveguide systems.

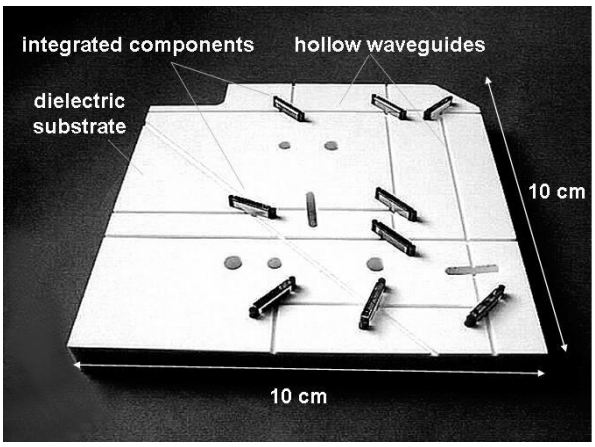

Fig.3. Photograph of a hollow waveguide based 10.6 μm lidar subsystem. The 10.6 μm radiation is guided through the circuit of components in the 2.0 mm cross-section hollow waveguides – a lid forms the forth (upper) wall of all the waveguides. The components include fully reflecting mirrors, beam splitters, Brewster plates etc.

As illustrated in figure 4 the subsystem was optically interfaced with laser sources, detectors and a telescope system in order to form a complete Range-Doppler imaging lidar. The figure also show measurements of the beam profile transmitted through the hollow waveguide circuit indicating how good the fundamental mode fidelity achieved in practice was. Figure 4 also shows a successful measurement of a Range-Doppler image of a re-entry vehicle target. Seperately, the homodyne detection efficiency of the subsystem was also measured. This yielded a value of 92% of the theoretical maxium. This emphasised how good the optical alignment that had been achieved in practice was.

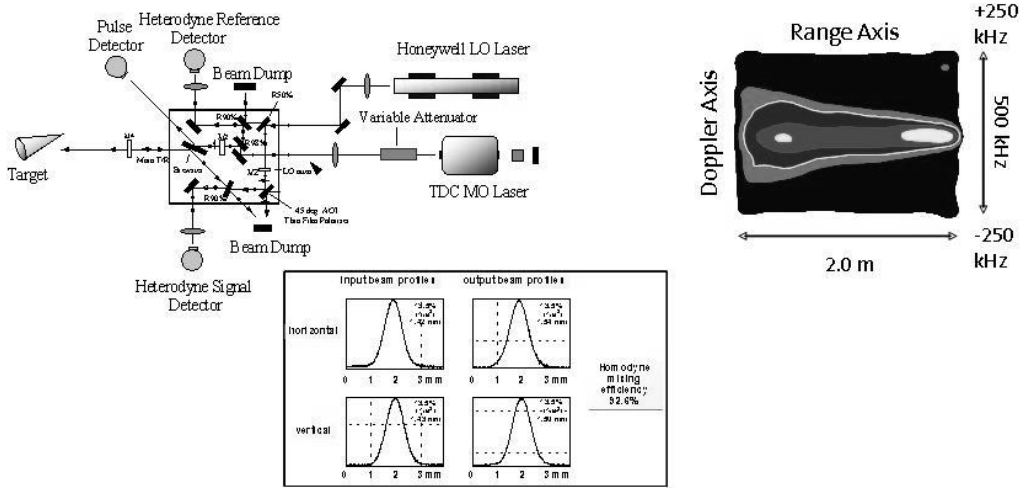

Fig.4. Schematic illustrating interfacing of the hollow waveguide subsystem with the master oscillator (MO) and local oscillator (LO) laser sources, detectors and the main transmit/receive telescope. Measurements of the transmitted beam fidelity – indicating good transmitted fundamental mode fidelity. An example of a measured Range-Doppler image of a re-entry vehicle target.

In relation to figures 3 and 4, it is also worth noting that the master oscillator was a mode-locked laser which generated a continuous train of pulses at an average power output of 20 watts. This power level was easily accomodated in the hollow waveguide circuit and power transmission levels in excess of 98% were measured for the longest optical path.

More recently under European Space Agency (ESA) funding the hollow waveguide integrated optic concept has been extended downwards in operational wavelength to 1.55 μm for space instrumentation applications. In this respect the goal of the work was to addresses the design, manufacture and assessment of: (i) a 1.55 μm coherent lidar circuit demonstrator, and, (ii) a 1.55 μm spectrometer circuit demonstrator. Based on the previously discussed design criteria aimed at achieving good fundamental mode propagation fidelity, the much shorter operational wavelength led to the choice of a 0.5 mm waveguide cross-section. This guide cross-section was used in conjunction with components that were 5.0 x 5.0 x 2.0 mm in dimension and alignment slots that were 4.0 mm deep. Once again the hollow waveguides and the component alignment slots were formed using precision computer controlled milling techniques. However, the shorter wavelength together with the 0.5 mm waveguide cross-section meant that Macor (a machinable glass-ceramic) could be used for the substrate whilst still providing very low waveguide attenuation coefficients. The use of Macor eased the challenges associated with the machining task. Based on these design and manufacturing concepts, as illustrated in figure 5, 1.55 μm lidar and spectrometer test circuits were manufactured. The combination of smaller cross-section waveguides and components led to demonstrator circuits with a footprint of only 40 x 40 mm. In the practical assessments, as with the earlier 10.6 μm work, the optical performance, including measurements of homodyne detection efficiency at 1.55 μm, were excellent for both systems.

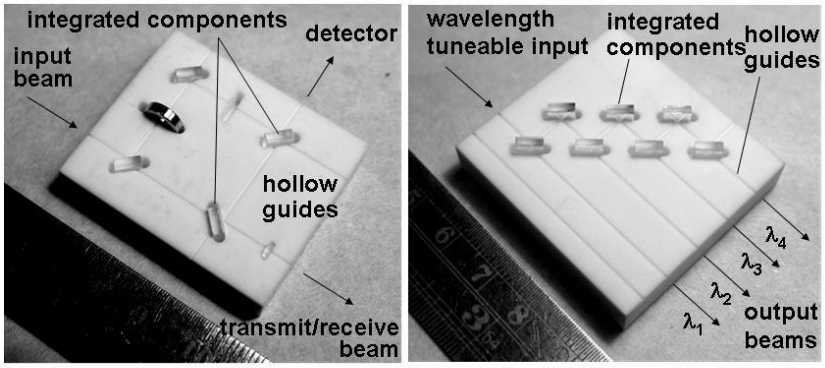

Fig.5. Photographs of 1.55 μm lidar and spectrometer test circuits based on 0.5 mm cross-section hollow waveguides in conjunction with 5.0 x 5.0 x 2.0 mm components in 4.0 mm deep alignment slots. Both demonstrator circuits are manufactured in Macor (glass-ceramic) substrates using precison computer controlled milling techniques.

The creation of hollow waveguide circuits is not limited to the use of computer controlled milling techniques. Laser machining, spark erosion, pressing and etching all have potential in conjunction with appropriate substrate materials. For example, figure 6 shows how MEMS microfabrication techniques based on deep reactive ion etching (DRIE) have been used in conjunction with silicon substrates to investigated the formation of hollow waveguides and component alignment slots [5-7]. The aim being to create a minaturized version of the concept in conjunction with micro-optical components. Figure 6 shows photographs of a component integration test array (left) and a 8.0 × 30.0 mm hollow silicon waveguide circuit chip (right). The fomer illustrates how 2.0 × 2.0 × 0.5 mm fully reflecting mirrors have been succesfully integrated into alignment slots in the silicon substrate to provide high fidelity fundamental mode transmission. Both chips are based on 125 μm cross-section hollow waveguides and are designed to operate at 1.55 μm. The 8.0 × 30.0 mm hollow silicon waveguide circuit chip (right) includes a range of discrete and monolithic components. On the upper left hand side of the chip a single mode fibre is held in position in a fibre guide with clips formed in the DRIE process. Efficient coupling from the 9 micron core single mode fibre to the 125 micron square hollow waveguide is to be achieved by the use of ball lens. The lens is integrated into the surface of the chip by location in a deeper alignment slot formed in a double etch depth process. A lid provides the fourth, upper wall of all the waveguides in question. The ultimate aim of this work is to create the optical equivalent of the electronic printed circuit board. Standard surface

mount technology could then be used for the automated manufacture of low cost hybrid modules. The approach could be applicable to: (i) optical telecomms modules (for both fibre and free-space comms) – Tx/Rx, EDFAs, Mux/Demux, MEMS VOAs and switches etc, (ii) interferometric sensors – displacement, motion etc, (iii) gas, vapour, liquid, chemical & biological sensors – lab-on-a-chip, (iv) direct and coherent detection lidar, and, (v) a range of military micro-optical systems – including hyperspectral sensors.

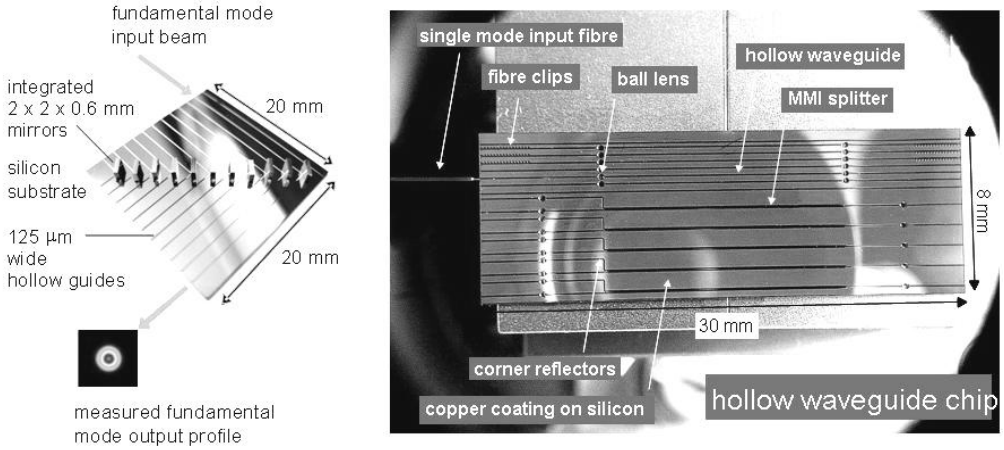

Fig.6. Photographs of hollow silicon waveguide circuit chips formed using deep reactive ion etchning (DRIE) techniques. The left hand photograph shows a 20.0 x 20.0 mm component integration test array. The right hand photograph shows an 8 x 30 mm hollow silicon waveguide circuit chip. The fomer illustrates how 2.0 x 2.0 x 0.5 mm fully reflecting mirrors have been succesfully integrated into alignment slots in the silicon substrate to provide high fidelity fundamental mode transmission. The latter illustrates how a range of discrete and monolithic components (including a single mode fiber and ball lenses) can be integrated together in order to provide the required optical circuit functionality.

Having provided some examples of the use of hollow waveguide circuits in the creation of compact, rugged, high performance, broad waveband electro-optic systems and subsystems we now turn our attention to individual hollow waveguide devices concepts.

4. HOLLOW WAVEGUIDE DEVICES

Whereas the hollow waveguide systems that have been described have focused on ensuring high fidelity fundamental mode propagation, the multimode propagation properties of hollow waveguides provide a rich source of optical functionality for individual devices [8-11]. Figure 7 illustrates an example of this in terms of a symmetric hollow waveguide based multimode interference (MMI) splitter. These devices have been realized in the hollow silicon waveguide technology described in the previous section. The symmetric MMI splitter simply takes the form of a square hollow input waveguide of cross-section a coupled symmetrically into a hollow rectangular waveguide of cross-section $a \times b$. In operation the square cross-section input waveguide is arranged to carry a fundamental mode field using the techniques described earlier in the paper. When this field enters the wider rectangular region it excites a spectrum of higher order modes. As predicted by equation (4), the different excited modes have different phase coefficients. As a result, as they propagate along the rectangular waveguide their relative phases, and the resultant transverse field intensity due to their superposition, changes. At certain well defined points along the axis of the hollow rectangular waveguide replications of the input field are produced. Figures 7a and 7b show a schematic and theoretical predictions for an N-way splitter. This has the rectangular waveguide section terminated with N output waveguides at an axial distance of $L = b^2/N\lambda$ [9]. Here λ is the free-space wavelength of the input radiation. It is interesting to note that putting $N = 1$, gives the length of rectangular waveguide that produces a single self-image of the input field, i.e. $L = b^2/\lambda$.

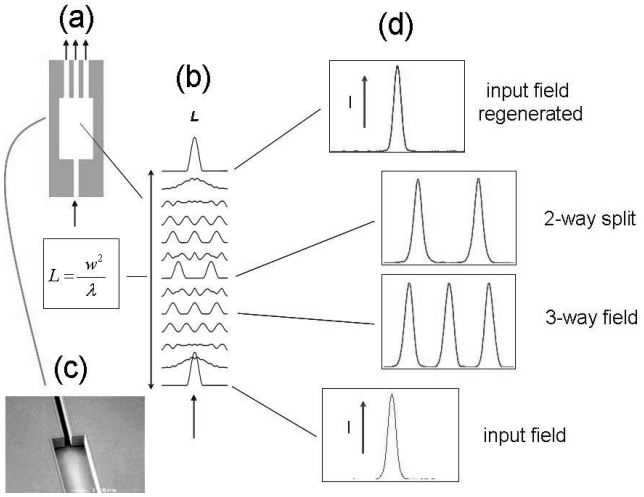

Fig.7. (a) schematic of symmetric hollow waveguide multimode interference (MMI) splitter, (b) theoretical line-profile predictions of the field in the rectangular guide, (c) SEM photograph of hollow silicon MMI splitter device, and, (d) experimental results for 1.55 μm input radiation and different lengths of the multimode waveguide region illustrating self-imaging of the input field and two-way and three-way splitting.

In practice, as illustrated in figures 7c and 7d, hollow waveguide MMI splitters were demonstrated with a 50.0 μm square input waveguide and a 250.0 μm wide by 50.0 μm high rectangular hollow waveguide [6]. With a rectangular guide width, b = 250.0 μm, and an operational wavelength of 1.55 μm, a self-image of the input field occurs with a rectangular guide length of, b^2/λ = 40.32 mm. A two-way power split is produced at half this length, i.e., at $b^2/2\lambda$ (20.16 mm), and, a three-way power split at one third this length, $b^2/3\lambda$ (13.44 mm).

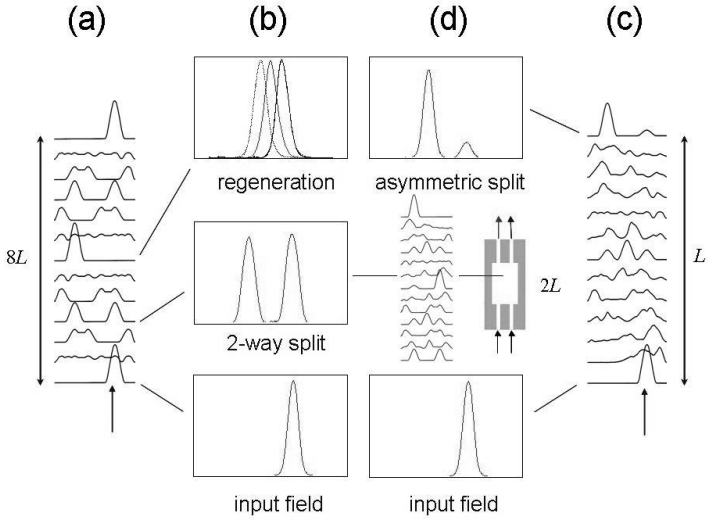

Figure 8. (a) & (c) theoretical line-profile predictions of the transverse field in the rectangular guide for an offset input waveguide, (b) & (d) experimental results for 1.55 μm input radiation and different lengths of the multimode waveguide region illustrating: (b) self-imaging & two-way symmetric splitting, and, (d) asymmetric splitting.

Figure 8 illustrates an analogous set of theoretical (figures 8a and 8c) and experimental (figures 8b and 8d) results for the case where the input waveguide (which carries a fundamental mode field) is laterally offset from the axis of the rectangular waveguide. This situation results in excitation of both symmetric and anti-symmetric modes in the rectangular waveguide and results in self-imaging of the input field at $L = 4b^2/\lambda$, and symmetric and asymmetric splitting

characteristics at $L = 4b^2/N\lambda$ and $L = 2b^2/N\lambda$, respectively. The theoretical plot in figure 8d, together with the inset schematic, shows the potential of using the 1-to-2-way splitter with offset input waveguides as the basis of a coherent mixer. Depending on the relative phases of the two fundamental mode input fields, output is produced at the left-hand (as illustrated) or right-hand output guide or is shared between them. In conjunction with a semiconductor laser source and a detector, an MMI mixer of this form is under consideration as the basis of an on-chip coherent lidar system.

The self-imaging and field splitting and mixing phenomena described above represent important functions for hollow silicon waveguide devices and circuits. A particular attraction in relation to the use of silicon microfabrication technology is that such devices can be formed at the same time, and in the same etch step, as the hollow waveguide circuit. This means that hollow waveguide MMI devices can take the place of discrete components. This leads to additional cost savings. A current limitation of the MMI devices is that they are relatively long. This is a consequence of the fact that the required length scales with the square of the width of the rectangular waveguide section. The width of the rectangular waveguide is determined by the widths of the square section input and output guides. The choice of widths for the input and output guides is dictated by the need to keep propagation losses suitably low. In further developments of the technology it is anticipated that coating techniques of the form used to improve the power transmission characteritics of hollow core light-pipes [12] will allow the reduction of input, output and multimode guide widths, and hence, the realisation of much shorter MMI devices.

5. CONCLUSIONS

The paper has described the use of hollow optical waveguides for both systems and devices. The use of hollow optical waveguide circuit boards (the optical PCB) to provide compact, rugged, high performance integrated optic systems and subsystems for both macro-optical and micro-optical components should prove very attractive. This is particularly the case where low cost, high volume, quality controlled manufacture is required. As demonstrated in the paper the fact that hollow waveguides can be designed for operation across a very broad wavelength range, and can support very high power propagation, adds to their usefulness. In conjunction with conventional pick-and-place equipment this new hybrid integration technology should facilitate low cost mass production of electro-optic systems for a wide range military applications. Conversely hollow waveguide multimode interference (MMI) devices form an important subset of components. As described in the paper these can provide a very wide range of intensity splitting, mixing and recombination functions. Wavelength multiplexing and demultiplexing functions are also feasible with suitable geometries. Most recently we have demonstrated multimode propagation phenomena in a hollow planar mirror waveguide as the basis of an interferometer with a fringe spacing of $\lambda/130$ [11].

REFERENCES

[1] E A J Marcatili, Bell Systems Technology Journal 48, 2103, (1969).
[2] K D Laakmann and W H Steier, Appl. Opt., 15, 1334, (1976).
[3] R M Jenkins, R Foord, A Blockley, T Papetti, D Graham and C Ingram, pp 4034-26, Proceedings of SPIE AeroSense Vol. 4034, Laser Weapons Technology Conference, 24th – 25th April 2000.
[4] R M Jenkins, R W J Devereux and A F Blockley, Jn. Mod. Opt. 45, 1613, (1998).
[5] R M Jenkins, M E McNie, Patent Application GB2003/000331, priority date 29th January 2002.
[6] R M Jenkins, M E McNie, A F Blockley, N Price, J McQuillan, Proc. European Conference on Optical Communications (ECOC), Paper Tu.1.2.4, Rimini (Italy), Sept 2003.
[7] M E McNie, R M Jenkins and A F Blockley, MicroTech 2004, Cambridge, UK.
[8] R Ulrich, Optics Comm. 13, 25, 1975.
[9] R M Jenkins, RW J Devereux, and J M Heaton, Opt. Lett. **17**, 991 (1992).
[10] R M Jenkins, RW J Devereux, and J M Heaton, Opt. Commun. **110**, 410 (1994).
[11] R M Jenkins, A F Blockley, J Banerji and Ar Davies, Phys. Rev. Lett. **100,** 163901 (2008)
[12] J A Harrington, Jn Fibre and Integrated Optics, 19, 211, (2000).

rmjenkins@qinetiq.com; office 44 (0)1684 895064, mobile 44 (0)7833 718602